SUPPLEMENTAL METHODS

Our supplement details pertinent methods used for geometry reconstruction from optical coherence tomography (OCT). In our description of reconstruction methods, we first describe the automated method of OCT frame analysis that uses image processing to detect and classify strut and lumen-vessel wall boundaries. Method validation is also provided.

OCT FRAME ANALYSIS

METHOD DEVELOPMENT

Fourier-domain OCT acquires scans at multiple depths (termed axial-line scans; A-lines) from an imaging wire that rotates inside a fluid-filled polymer tube(1). With one revolution (i.e. 360°), a complete cross-sectional frame can be acquired. At a pullback speed of 20mm/sec, up to 271 of these frames along the vessel length were acquired with distance of 50mm separating each segment length-wise. While stent struts and vessel borders are visualized on such OCT frames, the proprietary software accompanying the OCT system (LightLab Imaging Inc., Westford, Massachusetts) does not allow for the automated detection that was critical for our high processing needs. We therefore developed a method that automatically detects and classifies strut position and lumen borders from OCT frames. We did this by **classification** of features from A-line scans followed by **edge detection** of the signal within the A-line.

Classification: A-lines were classified as belonging to strut or lumen using features extracted from the "scale-space signature" of the signal. This signature was generated by convolving the 1-D A-line signal, $f(r)$ where r is the axial distance, by a mother wavelet $\psi(r)$

$$Wf(s,r) = \frac{1}{s}\int f(r)\psi\left(\frac{r-a}{s}\right)dx. \quad (1)$$

Here *a* and *s* are the shift and scale parameters, respectively. The scale space signature of the A-line signal is the local maximum of the wavelet transform with the Laplacian-of-Gaussian (LoG) wavelet at each scale $s = \{0: 2^{0.1}: 2^{8}\}$, referred as the "LoG response". Tsantis et al.(2) have demonstrated that the LoG response of metallic struts are characteristically different to that of tissues (Supplement Figure 1B). We similarly extracted features from the LoG response (Supplemental Table 1) and used these features to train a machine learning model based on a decision tree algorithm (Bootstrap aggregation) to classify the A-line signal into three groups: (1) strut and (2) lumen and (3) "other" structures (residual blood).

Table 1: Table of Extracted Features used to classify lumen and stent strut structures in OCT images

Features Derived from Wavelet Transform
Scale s=s*, location of maximum Log Response
Maximum LoG Response max [illegible]

Position on radial axis of maximum LoG Response at scale s=s*
Standard deviation of LoG Response
Mean LoG Response
Skew of LoG Response
Position on radial axis of maximum DoG Response at scale s=s*
Signal Features
Max(signal)
Mean (signal)
Neighbourhood Features
s* of four closest neighbours

As the guidewire is metallic and has a similar scale space signature as "struts", a semi-automated approach was used to avoid misclassification errors. Briefly, the guidewire was selected manually on the first frame, and then a minimum spanning tree algorithm automatically identified the guidewire on each subsequent slice along the pullback length. Entities initially classified as "struts" but characterized as "guidewire" based on this algorithm were reclassified as "other".

Edge detection: Once A-lines had been classified, edge locations of the strut and lumen were obtained using another wavelet transformation (akin to a Canny edge detector(3)). Edges of the strut (abluminal side) and lumen/tissue interface represent a step edge. To optimally detect these edges, the A-line signal was convolved with the normalized first derivative of the Gaussian wavelet. This wavelet has a characteristic scale s^* taken from the LoG response for either strut or lumen classification noted above. A-lines classified as "other" were not considered. Adjacent strut pixels in the polar image were clustered using connected components labeling(4), and each cluster's centroid was used to define a single pixel defining abluminal strut surface position (as designated by the red cross in Supplemental Figure 1C). . Lumen pixel candidates were interpolated and smoothed to generate a closed lumen border (as designated by the green boundary in Supplemental Figure 1C). Strut surface pixels and lumen border pixels were transformed into Cartesian coordinates. The true centroid of the 2D strut was obtained by projecting the strut surface position by half a strut width in the direction of the vessel wall.

VALIDATION

Accuracy of extracted strut and lumen dimensions was computed using a candidate data set in the LCX vessel of a single pig. Each A-line within the stented segment of 80 slices (≈40100 A-line signals) was classified as belonging to strut, lumen or "other" categories (including contrast or artifacts in the tissue). A classifier was trained with these categories as outputs and the extracted features of the A-line signal from the wavelet transform as the inputs. Receiver-operator characteristic curves showed an area under the curve (AUC) measurement for classification of strut candidates to be 0.99, the lumen ~1.0 and for "other" structures 0.99, with

sensitivity and specificity values ranging from approximately 0.94-1.0 and 0.83-0.99, respectively (Supplemental Figure 1C). This method of feature detection had a 10-fold cross-validation rate of 99.8% in successfully predicting strut classes, and a 99.2% and 97.8% rate for lumen and "other" structures, respectively.

As a secondary confirmation, comparisons were made in area measurements with the proprietary software (LightLab Imaging Inc., Westford, Massachusetts). Manual tracings of stent and lumen were made by a trained operator in three stented vessels in a different animal than that was used to train the automated classifier. Lumen area was calculated as the integrand of the radial location of the lumen boundaries in the Cartesian image while the stent area was calculated from a circle fitted to the detected stent struts within each frame (frames with less than one detected strut per quadrant were discarded). Differences in area measurements between the manual and automated methods are presented in the text as mean ± standard deviation, along with linear regression analysis and their respective Pearson correlation coefficients.

SUPPLEMENTAL FIGURES

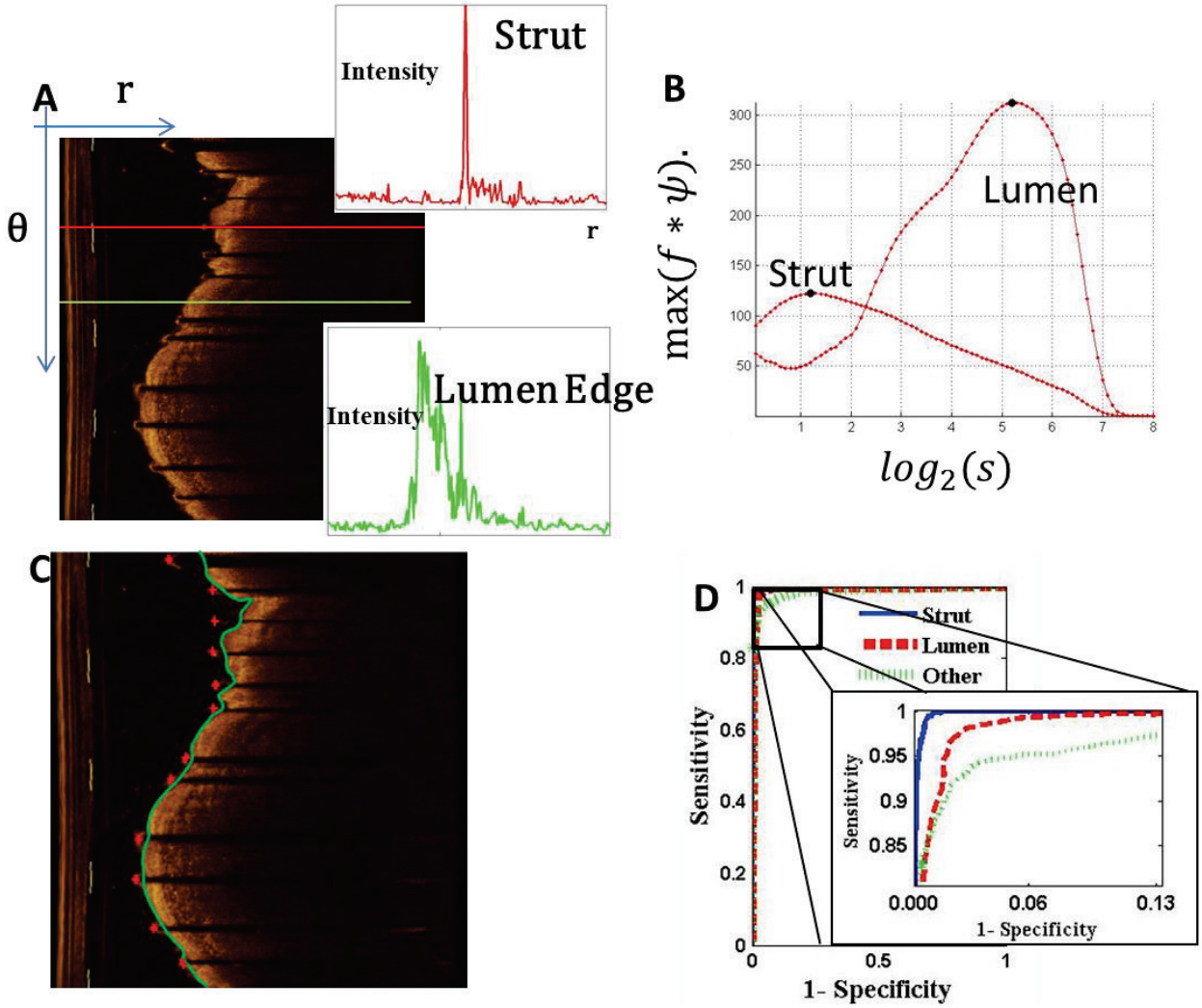

Supplemental Figure 1: (A) Example of an optical coherence image in the polar coordinate system. A pixel stent strut candidate creates a trailing shadow in its A-line, when compared to a pixel candidate belonging to the lumen wall. (B) The convolution of each A-line signal with the negative normalized second-derivative of the Gaussian yields the LoG response across scales, and this coarse-to-fine tracking is called the scale space signature. Using features extracted from the scale space signature, one can classify structures as part of either (C) lumen (-) or stent strut (+). (D) Receiver operator characteristic curves illustrate the accuracy in classifying lumen and strut structures from the derived feature set and using a decision tree algorithm (Bootstrap aggregation).

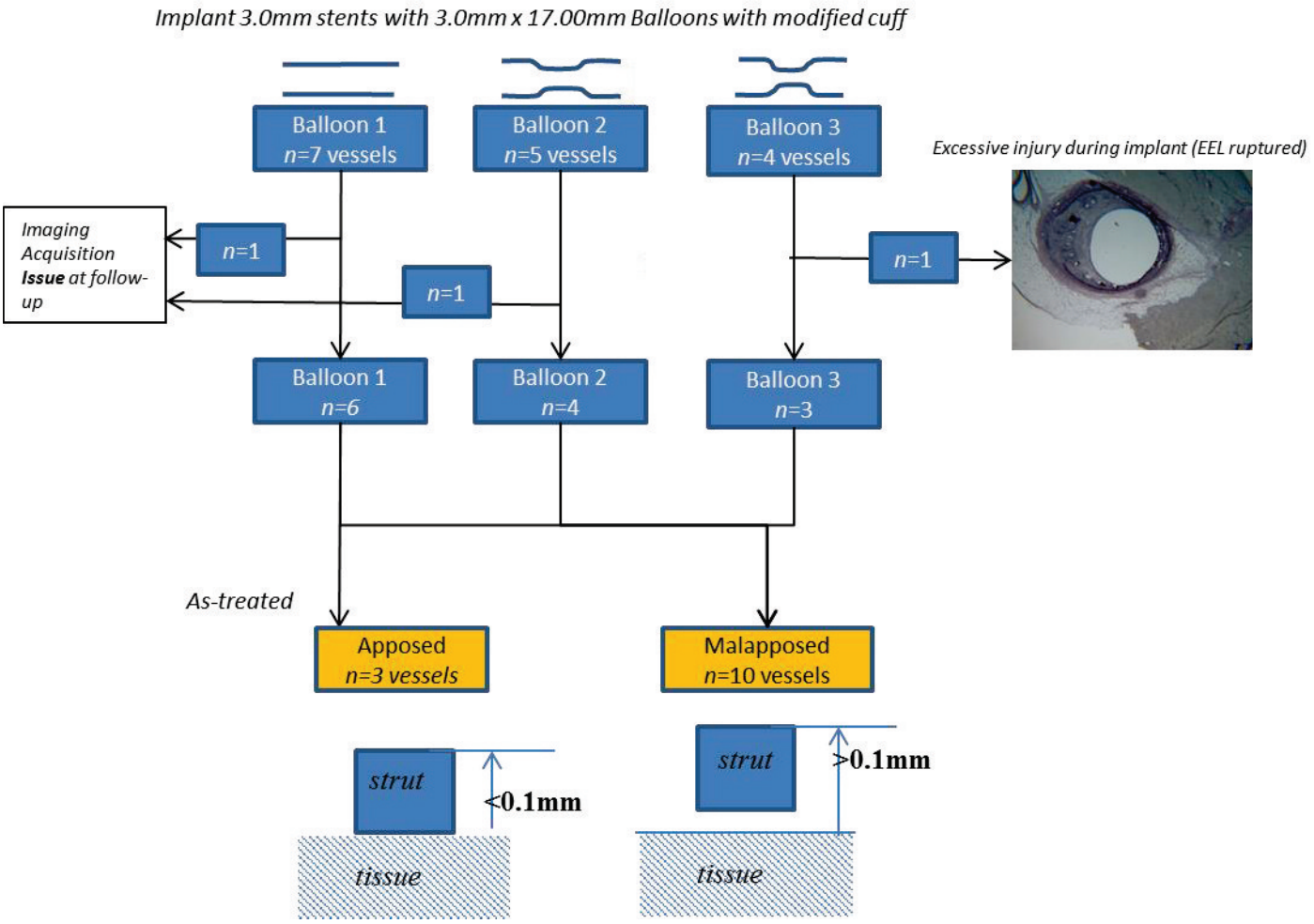

Supplemental Figure 2: Study Design

SUPPLEMENTAL REFERENCES

1. Bezerra H. G., M. A. Costa, G. Guagliumi, A. M. Rollins, D. I. Simon. Intracoronary optical coherence tomography: a comprehensive review clinical and research applications. JACC Cardiovasc Interv 2009;2:1035-46.

2. Tsantis S., G. C. Kagadis, K. Katsanos, D. Karnabatidis, G. Bourantas, G. C. Nikiforidis. Automatic vessel lumen segmentation and stent strut detection in intravascular optical coherence tomography. Med. Phys. 2012;39:503-13.

3. Zhang L., P. Bao. Edge detection by scale multiplication in wavelet domain. Pattern Recognition Letters 2002;23:1771-1784.

4. Haralick R. M., L. G. Shapiro. Computer and Robot Vision: Addison-Wesley Longman Publishing Co., Inc., 1992.